J. Fluid Mech. (2012), *vol.* 712, *pp.* 219–243.
doi:10.1017/jfm.2012.413

Spontaneous formation of travelling localized structures and their asymptotic behaviour in binary fluid convection

Takeshi Watanabe[1]†, **Makoto Iima**[1] **and Yasumasa Nishiura**[2]

[1] Department of Mathematical and Life Sciences, Graduate School of Science, Hiroshima University, 1-7-1 Kagamiyama, Higashi-Hiroshima, Hiroshima 739-8521, Japan

[2] WPI Advanced Institute for Materials Research, Tohoku University, 2-1-1 Katahira, Aoba-ku, Sendai 980-8577, Japan

(Received 11 October 2011; revised 13 July 2012; accepted 16 August 2012; first published online 28 September 2012)

We study spontaneous pattern formation and its asymptotic behaviour in binary fluid flow driven by a temperature gradient. When the conductive state is unstable and the size of the domain is large enough, finitely many spatially localized time-periodic travelling pulses (PTPs), each containing a certain number of convection cells, are generated spontaneously in the conductive state and are finally arranged at non-uniform intervals while moving in the same direction. We found that the role of PTP solutions and their strong interactions (collision) are important in characterizing the asymptotic state. Detailed investigations of pulse–pulse interactions showed the differences in asymptotic behaviour between that in a finite but large domain and in an infinite domain.

Key words: absolute/convective instability, bifurcation, double diffusive convection

1. Introduction

Rayleigh–Bénard convection is one of the most well-known examples of pattern-formation phenomena: depending on the parameters, convection cells form various patterns including rolls or hexagons (Busse 1964). In many convection experiments (Heinrichs, Ahlers & Cannell 1987; Kolodner, Bensimon & Surko 1988; Niemela, Ahlers & Cannell 1990; Kolodner 1991), a long narrow channel has been used to mimic a two-dimensional situation. In such a situation, convection rolls which are uniform in the roll axis direction are observed, which can be modelled by two-dimensional flow. Under the two-dimensional assumption, only a stationary overturning convection (SOC) is possible in a (pure-fluid) Rayleigh–Bénard convection near and above critical temperature gradient. However, in a mixture of two miscible fluids such as water and ethanol (binary fluid), richer convection patterns can be observed even in two-dimensional space, in addition to an SOC. In this paper we focus in particular on a class of spatially localized convective patterns called 'pulses' and study their role in the asymptotic behaviour for $t \to \infty$.

The rich patterns in binary fluids are explained by the Soret effect (Platten 2006), by which a concentration gradient is induced by a temperature gradient. In some cases, including appropriately proportioned water–ethanol mixtures, the concentration and

† Email address for correspondence: wtakeshi@mis.hiroshima-u.ac.jp

temperature gradients have opposite effects on the buoyancy: convection is motivated by the temperature gradient but inhibited by the concentration gradient. As a result, the critical Rayleigh number Ra_c, at which the conductive state loses stability, becomes larger than that of pure-fluid Rayleigh–Bénard convection. In this case, a bistable region between the conduction state and the convection state is typically observed.

Such bistability has been related to the spatially localized solutions (pulse solutions). A pair of 'pinning' fronts connecting to two stable states leads to the bound state, which corresponds to the pulse solutions (Pomeau 1986). Recently, more detailed studies of bistable systems for the pulse solution and the structure of snaking bifurcation have been published (Burke & Knobloch 2007; Beck *et al.* 2009; Chapman & Kozyreff 2009). Therefore the relationship between the bistable region and spatially localized solutions in binary fluid convection is of great interest. A 'convecton' (Batiste *et al.* 2006), or a steady pulse (SP), is a spatially localized solution in binary fluid convection that is steady in time. The SP solution was obtained numerically by Batiste *et al.* (2006). They presented a branch of the SP solution with a snake-like structure known as 'homoclinic snaking' (Woods & Champneys 1999; Burke & Knobloch 2007), which has subsequently been observed in some other systems (Burke & Knobloch 2006; Schneider, Gibson & Burke 2010; Houghton & Knobloch 2011).

There emerges another interesting type of spatially localized pattern: periodic travelling pulses (PTPs), i.e. moving spatially localized convection cells whose shapes periodically change with time. Note that the same structure is also called by other names, e.g. travelling-wave pulse (or TW pulse) (Kolodner 1991) or localized travelling wave (or LTW) (Niemela *et al.* 1990; Ning, Harada & Yahata 1996; Jung, Matura & Lücke 2004). However, we use the term PTP so as to emphasize the time-periodicity in the reference frame. Here we investigate in particular the spontaneous formation of PTPs and their asymptotic behaviour for $t \to \infty$ in large periodic domains when the conductive state is unstable.

PTPs were first experimentally observed by Heinrichs *et al.* (1987) as a transient state for a steady localized travelling wave alongside the sidewall of the container, and the origin of the localization was explained by the sidewall effect predicted by Cross (1986). However, PTPs were also observed in an annulus by Kolodner *et al.* (1988), so the sidewall effect is not necessary to account for the localization mechanism. Thual & Fauve (1988) then provided a theoretical model in terms of the Ginzburg–Landau equation (GL) in a periodic domain, and found that the mechanism for localized states is not attributed to the sidewall effect but to the non-variational effect of the system. Their theory was experimentally supported by Niemela *et al.* (1990), who compared PTP states in a rectangular container with those in an annular container and showed that the PTP state is qualitatively geometry-independent. After their experiments, many authors conducted convection experiments in annular containers under various parameters. In particular, Kolodner's experiment (Kolodner 1991) is interesting because he showed that the group velocity of PTPs varies according to the Rayleigh number.

The GL approach was extended to a general framework by van Saarloos & Hohenberg (1992), focusing on the pattern selection of coherent structures. Recently, Iima & Nishiura (2009) addressed the collision process of two counter-propagating PTPs via extended complex GL. Although their results reproduced the experiment performed by Kolodner (1991) qualitatively, a study based on the Navier–Stokes equations should be considered because the structure of PTPs cannot be resolved by amplitude equations such as GL and related equations. A PTP consists of a certain

number of moving convection cells within its envelope. Therefore, understanding the detailed collision process requires the internal dynamics of convection cells of PTPs.

A Navier–Stokes approach has also been conducted by many authors (Barten, Lücke & Kamps 1991; Barten *et al.* 1995; Ning *et al.* 1996; Jung *et al.* 2004; Toyabe 2009). For example, Barten *et al.* (1995) and Jung *et al.* (2004) performed time evolution studies in two-dimensional space in a parameter range in which both conduction and travelling-wave solutions are stable. They obtained PTPs as an asymptotic state. Because PTPs contain internal dynamics of generating and destroying convection cells within the envelope, we need to obtain a PTP as a solution satisfying appropriate mathematical conditions. In fact, Toyabe (2009) studied the collision problem of PTPs obtained by the asymptotic states, and found that the result was sensitive to the detailed change of parameters. Recently, Watanabe *et al.* (2010) succeeded in obtaining PTPs globally in parameter space as a time-periodic travelling solution numerically. Further, they constructed the bifurcation branch of the PTP solutions. The branch has saddle-node points, but the shape is not snaky as is often observed for spatially localized structures including 'convectons' (Batiste *et al.* 2006). The PTP solution is useful for detailed analysis such as control of the precise initial conditions including the internal state of convection cells, which will be presented in detail in this paper.

Remarkably, stable SP branches exist in small domain sizes with periodic boundary condition even when the conductive state is unstable (Batiste *et al.* 2006; Mercader *et al.* 2011), which is also true for PTP solutions (Watanabe *et al.* 2010). This phenomenon for PTPs was reproduced in an experiment conducted by Niemela *et al.* (1990) in an annular container. They explain this fact in terms of the convective/absolute instability. In such a situation, perturbation growth in a convectively unstable region can be suppressed because perturbations are absorbed at the front of the pulse if their amplitude is not too large. In other words, even if the background state (conductive state) is convectively unstable, pulse solutions can persist provided that the domain is not too large.

Now, the following natural question arises: What is the final asymptotic state in binary fluid convection for a large but finite domain when the background (conductive) state is convectively unstable? If the system is large enough, the perturbations can grow sufficiently large to form convection cells and may destroy the various pulse solutions even if they are stable in smaller domains.

Consider the time evolutions starting from small-amplitude perturbations in a large periodic domain, as shown in figure 1 (cf. § 5), where the aspect ratio of the computational domain Γ is 500. In both cases, small initial perturbations grow to form some coherent structures. After a series of complicated transition processes, we see an array of PTPs moving in the same direction with non-uniform intervals.

It is worth considering this asymptotic state, focusing on the lengths of conduction regions between arranged PTPs. As is pointed out above, perturbations are absorbed by PTPs, and thus PTPs are approximately 'impermeable' for disturbances. Therefore, a large unstable conduction state at $t = 0$ (see figure 1) is finally divided into small partitions by PTPs. Although perturbations could grow sufficiently at the early stage because the unstable conductive state is long enough for disturbances to grow, they no longer do so at $t \gg 1$ because they are promptly absorbed at the nearest PTP in the propagating direction. This point is argued in detail in § 6.1.

Strong interactions (collisions) between localized structures have an important role in transition processes and have been extensively investigated, for example, in barchan dunes (Katsuki *et al.* 2005), reaction–diffusion systems (Nishiura, Teramoto & Uera 2003*b*; Teramoto, Ueda & Nishiura 2004; Nishiura, Teramoto & Ueda 2005), and

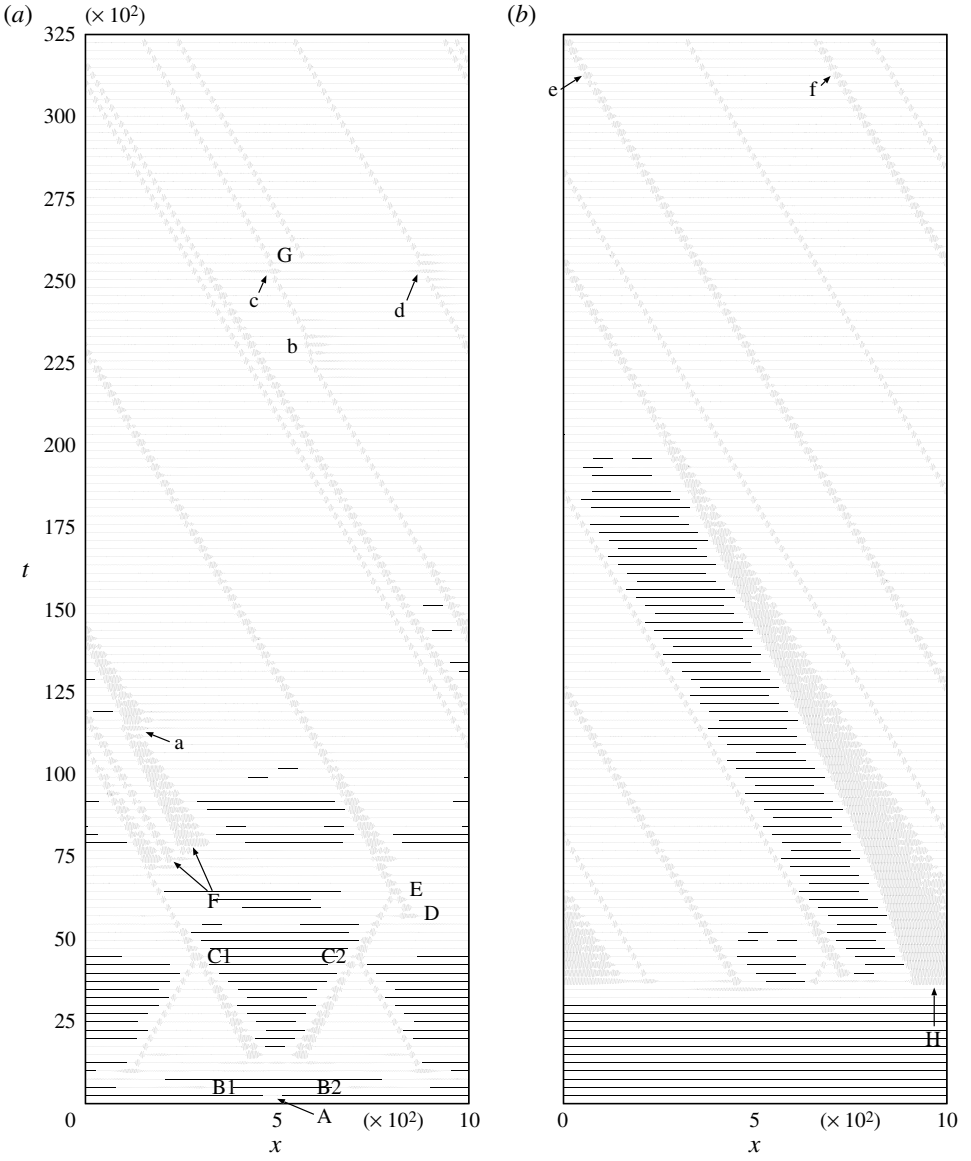

FIGURE 1. Time evolution of $\psi(x, 0, t)$ for $\Gamma = 500$. (*a*) A point disturbance is added at $t = 0$, $x = 500$, and (*b*) small random disturbances are added across the whole domain. The time interval of the visualization is $t = 250$. Note that the size of the periodic box is $2\Gamma = 1000$. In both figures, each localized structure except e and f, for $t \gtrsim 27\,500$, corresponds to a PTP solution in figures 3, 5 and 6(*b,d*); e and f correspond to figure 6(*a,c*). Each collision process (C1, C2 and E) resembles figure 11(*a*). See § 5 for details.

the Swift–Hohenberg equation (Houghton & Knobloch 2011). In the present case, the role of collisions between counter-propagating PTPs is also very important. In fact, PTP–PTP collision has been examined experimentally (Kolodner 1991), showing that the collision results depend on the velocity of each pulse: they fuse into a single PTP when the PTP velocity is large, but bind at a distance when the velocity is small. The

result of a collision also depends on the phase of each PTP at the instant of collision because PTPs are time-periodic in a moving frame. This phase dependence of PTP collisions was first studied by Toyabe (2009) and more recently by Watanabe *et al.* (2010) in greater detail.

The main theme of this paper is a pattern formation mechanism in binary fluid convection when the conductive state is unstable. In particular, we clarify the dependence of the asymptotic pattern for $t \to \infty$ on system size. Our conjecture is that the asymptotic pattern is an array of unequally distanced PTPs for generic initial data, when the domain is large but finite. To show this, we first list the possible localized structures, including SPs, PTPs and PTP-like structures, that have not been reported. Then we clarify the maximum and minimum domain size for a single PTP. At the maximum domain size, we find that the single PTP solution disappears via the saddle-node bifurcation. Further, we study the interactions among pulses. It is shown that PTPs have strong survival ability, which supports the numerical time evolution results obtained with generic initial conditions. These results suggest the existence of three qualitatively different system sizes:

(i) small (a solitary PTP exists);

(ii) large enough but finite (a solitary PTP cannot exist);

(iii) infinite.

Our main concern in the present study is to clarify case (ii) in detail. Although phenomena which occur in case (iii) are not necessarily clear, the patterns formed are expected to be completely different from case (ii), because wave-packet disturbances and pulses moving in an arbitrary direction can always appear somewhere in the system and therefore there may arise no modulated direction.

Here we would like to stress the importance of numerical solutions to study of the pattern formation problem. To investigate the pattern formation phenomena it is essential to know the behaviour of possible patterns in global parameter space including unstable ones and, further, it is not until we know the PTP solution that we can examine the phase dependence of PTP–PTP collisions accurately (see § 6.3) – not to mention the importance of the solution itself.

This paper is organized as follows. In § 2 we introduce the basic equations, and in § 3 we review numerical schemes for obtaining the various classes of solutions. Then § 4 presents a detailed bifurcation diagram for a relatively small aspect ratio ($\Gamma = 32$). The main focus is then addressed in § 5, where the domain-size dependence of the pattern formation process is discussed. Time evolutions starting from generic initial conditions are described, and the critical Γ for a single PTP is obtained. In § 6, we focus on pulse–pulse interactions, that is, collisions between counter-propagating PTPs, interactions between co-propagating PTPs, and SP–PTP collisions. These processes are fundamental to our understanding of the complete asymptotic dynamics.

2. Basic equations

Consider a two-dimensional binary-fluid layer confined between two horizontal plates as shown in figure 2. The governing equations for the binary fluid convection are given as follows (Platten & Legros 1984):

$$\tilde{\boldsymbol{\nabla}} \cdot \tilde{\boldsymbol{u}} = 0, \tag{2.1}$$

$$\frac{\partial \tilde{\boldsymbol{u}}}{\partial \tilde{t}} + (\tilde{\boldsymbol{u}} \cdot \tilde{\boldsymbol{\nabla}})\tilde{\boldsymbol{u}} = -\frac{1}{\rho_0}\tilde{\boldsymbol{\nabla}}\tilde{p} + \nu\tilde{\nabla}^2\tilde{\boldsymbol{u}} + \{\alpha(\tilde{T} - T_0) - \beta(\tilde{C} - C_0)\}g\boldsymbol{j}, \tag{2.2}$$

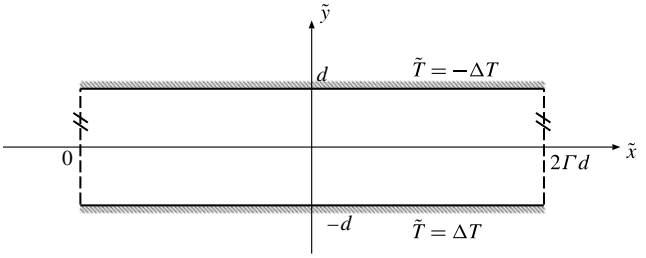

FIGURE 2. System configuration.

$$\frac{\partial \tilde{T}}{\partial \tilde{t}} + (\tilde{\boldsymbol{u}} \cdot \tilde{\nabla})\tilde{T} = \kappa \tilde{\nabla}^2 \tilde{T}, \tag{2.3}$$

$$\frac{\partial \tilde{C}}{\partial \tilde{t}} + (\tilde{\boldsymbol{u}} \cdot \tilde{\nabla})\tilde{C} = \gamma_2 \tilde{\nabla}^2 \tilde{T} + D\tilde{\nabla}^2 \tilde{C}, \tag{2.4}$$

where $\tilde{\boldsymbol{u}} = (\tilde{u}, \tilde{v}, \tilde{w})$ is the velocity of the fluid, $\tilde{t}$ is the time, ρ_0 is the mean density of the mixture, $\tilde{p}$ is the pressure, ν is the kinematic viscosity, α is the coefficient of thermal expansion, $\tilde{T}$ is the temperature, T_0 is the reference temperature, β is the coefficient of variation in the concentration of the mixture, $\tilde{C}$ is the concentration, C_0 is the reference concentration, g is the gravitational acceleration, $\boldsymbol{j}$ is the unit vector in the $\tilde{y}$-direction, κ is the thermal diffusivity, D is the concentration diffusivity, and γ_2 is the coefficient of the Soret effect. Note that, in this paper, dimensional variables are denoted by an added $\tilde{}$. A periodic boundary condition with period $2\Gamma d$ is imposed in the $\tilde{x}$-direction.

Equation (2.1)–(2.4) can be rewritten as

$$\frac{\partial}{\partial t}\left(\nabla^2 \psi\right) = \frac{\partial(\psi, \nabla^2 \psi)}{\partial(x, y)} + \sigma \nabla^4 \psi - \frac{\sigma Ra}{16}\left\{(1+S)\frac{\partial \theta}{\partial x} - S\frac{\partial \eta}{\partial x}\right\}, \tag{2.5}$$

$$\frac{\partial \theta}{\partial t} = \frac{\partial(\psi, \theta)}{\partial(x, y)} - \frac{\partial \psi}{\partial x} + \nabla^2 \theta, \tag{2.6}$$

$$\frac{\partial \eta}{\partial t} = \frac{\partial(\psi, \eta)}{\partial(x, y)} + \nabla^2 \theta + Le\nabla^2 \eta, \tag{2.7}$$

where σ is the Prandtl number, Ra is the Rayleigh number, Le is the Lewis number, and S is the separation ratio defined by

$$\sigma = \frac{\nu}{\kappa}, \quad Ra = \frac{16\alpha g d^3 \Delta T}{\kappa \nu}, \quad Le = \frac{D}{\kappa}, \quad S = \frac{\beta \gamma_2}{D\alpha}. \tag{2.8}$$

Here ψ is the stream function such that $u = \partial\psi/\partial y$, $v = -\partial\psi/\partial x$, and all the variables are represented in non-dimensional form:

$$\tilde{\boldsymbol{u}} = \frac{\kappa}{d}\boldsymbol{u}, \quad (\tilde{x}, \tilde{y}) = d(x, y), \quad \tilde{t} = \frac{d^2}{\kappa}t, \quad \tilde{p} = \frac{\rho_0 \kappa^2}{d^2}p, \tag{2.9}$$

$$\tilde{T} - T_0 = \Delta T(\theta - y), \quad \tilde{C} - C_0 = \frac{\gamma_2 \Delta T(\eta - \theta + y)}{D}. \tag{2.10}$$

Note that the separation ratio S denotes the strength of the Soret effect and can take both positive and negative values according to the sign of γ_2. However, we

assume S to be negative in the present study, which means that the Soret effect inhibits convection. If the sign were positive instead, the flow would be completely different because the concentration field also motivates convection (Platten 2006).

Throughout this paper, we use Kolodner's experimental parameters (Kolodner 1991), $Le = 0.0088$, $\sigma = 7$, and $S = -0.123$, because PTPs are observed in this parameter. The boundary conditions in the y-direction are

$$\frac{\partial \psi}{\partial y}(x, \pm 1, t) = \theta(x, \pm 1, t) = \frac{\partial \eta}{\partial y}(x, \pm 1, t) = 0, \quad \psi(x, \pm 1, t) = \psi_c(\pm 1, t), \tag{2.11}$$

and a periodic boundary condition with period 2Γ is imposed in the x-direction. Then, the calculation was performed for a $[-1, 1] \times [0, 2\Gamma)$ domain. The control parameter is the Rayleigh number Ra and the aspect ratio Γ. Note that $\psi(x, \pm 1, t)$ is not zero because the spatially averaged velocity is allowed to have an x-component and $\psi_c(\pm 1, t)$ is determined automatically in the calculation (see § 3).

3. Numerical method

The spectral method was used for the numerical solution of (2.5)–(2.7) as follows:

$$\begin{pmatrix} \psi(x, y, t) \\ \theta(x, y, t) \\ \eta(x, y, t) \end{pmatrix} = \sum_{l=-[L/2]}^{[(L-1)/2]} \mathrm{e}^{\mathrm{i}klx} \begin{pmatrix} \psi_l(y, t) \\ \theta_l(y, t) \\ \eta_l(y, t) \end{pmatrix}, \quad \begin{pmatrix} \psi_l(y, t) \\ \theta_l(y, t) \\ \eta_l(y, t) \end{pmatrix} = \sum_{m=1}^{M} \begin{pmatrix} \Psi_m^{(l)}(y)\psi_{lm}(t) \\ \Theta_m(y)\theta_{lm}(t) \\ H_m(y)\eta_{lm}(t) \end{pmatrix}, \tag{3.1}$$

where $k = \pi/\Gamma$ is the wavenumber, i is the imaginary unit, L and M are truncation numbers, and $\Psi_m^{(l)}(y)$, $\Theta_m(y)$, and $H_m(y)$ are defined in terms of the Chebyshev polynomial $T_m(y) = \cos(m \cos^{-1}(y))$ as

$$\Psi_m^{(l)} = \begin{cases} (1 + a_m y^2 + b_m y^4) T_m - \cos \dfrac{m\pi}{2} & (l = 0), \\ (1 - y^2)^2 T_{m-1} & (l \neq 0), \end{cases} \tag{3.2}$$

$$\Theta_m = (1 - y^2) T_{m-1}, \tag{3.3}$$

$$H_m = \frac{1}{2\{(m+1)^2 - 1\}} \left\{ (1 - y^2) T''_{m+1} + 2y T'_{m+1} - 2T_{m+1} \right\}, \tag{3.4}$$

to satisfy the boundary conditions (2.11), where a_m and b_m are determined so as to satisfy the conditions

$$\left. \frac{\mathrm{d}\Psi_m^{(0)}}{\mathrm{d}y} \right|_{y=\pm 1} = \left. \frac{\mathrm{d}^3 \Psi_m^{(0)}}{\mathrm{d}y^3} \right|_{y=\pm 1} = 0. \tag{3.5}$$

Note that the boundary condition for $l = 0$ is different from the others because $\psi_c(\pm 1, t)$ in (2.11) corresponds to the Fourier coefficient for $l = 0$, i.e. substituting $l = 0$ and $y = \pm 1$ into ψ in (3.1) we have

$$\psi(x, \pm 1, t) = \sum_{m=1}^{M} \Psi_m^{(0)}(\pm 1) \psi_{0m}(t) = \psi_c(\pm 1, t) \tag{3.6}$$

and thus $\Psi_m^{(0)}(\pm 1)$ should not be zero. In other words, $v = -\partial\psi/\partial x$ is identically zero because $[-\partial\psi/\partial x]_l = \mathrm{i}kl\psi_l = 0$ when $l = 0$, and thus we cannot adopt the condition $\psi(\pm 1, t) = 0$ as the boundary condition in this case. Then we consider

the x-component of the Navier–Stokes equations:

$$\frac{\partial u}{\partial t} + (\boldsymbol{u} \cdot \nabla)u = -\frac{\partial p}{\partial x} + \sigma \left(\frac{\partial^2 u}{\partial x^2} + \frac{\partial^2 u}{\partial y^2} \right). \tag{3.7}$$

The l-component of the equation above is

$$\frac{\partial u_l}{\partial t} + [(\boldsymbol{u} \cdot \nabla)u]_l = -\mathrm{i}klp_l - \sigma k^2 l^2 u_l + \sigma \frac{\partial^2 u_l}{\partial y^2}. \tag{3.8}$$

Thus, only the contribution of the third term of the right-hand side is retained on the two walls when $l = 0$, and we have

$$0 = \sigma \left. \frac{\partial^2 u_0}{\partial y^2} \right|_{y=\pm 1}, \tag{3.9}$$

and therefore the boundary condition for $l = 0$ (3.5) is obtained. Note also that the $(l = 0)$-component is zero for SP solutions and not zero for PTP solutions, although the contribution is very small.

Equation (3.1) is substituted into (2.5)–(2.7) and the collocation method is applied; then, $3LM$ simultaneous ordinary differential equations are obtained. Thus, the equations can be simply described by

$$\frac{\mathrm{d}\boldsymbol{z}}{\mathrm{d}t} = \boldsymbol{f}(\boldsymbol{z}), \tag{3.10}$$

where

$$\boldsymbol{z} = \{z_{lmn}\} \quad (l = 1, 2, \ldots, L;\ m = 1, 2, \ldots, M;\ n = 1, 2, 3) \tag{3.11}$$

and $(z_{lm1}, z_{lm2}, z_{lm3}) = (\psi_{lm}, \theta_{lm}, \eta_{lm})$. The flow $\boldsymbol{\phi} = \{\phi_{lmn}\}$ given by the vector field $\boldsymbol{f}$ is defined as

$$z(t) = \boldsymbol{\phi}(z^{(0)}, t), \tag{3.12}$$

where $\boldsymbol{\phi}(z^{(0)}, 0) = z^{(0)}$. Collocation points are chosen to be extrema of the Chebyshev polynomials, which has an advantage in resolving steep variation of concentration boundary layer near both walls.

The phase-space vector $\boldsymbol{z}$ is integrated numerically using the forward Euler method together with the Crank–Nicolson method for viscous and diffusion terms and the Adams–Bashforth method for nonlinear terms. The truncation number M is chosen to be $M = 32$, and L is the smallest odd non-prime number that satisfies $L > 16\Gamma$.

The Newton–Raphson method can be used to find the solutions in table 1 by calculating the fixed point of the Poincaré section together with the GMRes method (Watanabe *et al.* 2010). Further, the Arnoldi method can be utilized to solve eigenvalue problems to examine the linear stability of the solutions.

The numerical accuracy is examined by increasing the truncation numbers L and M. For example, period τ and translation $U\tau$ for the PTP solution for $Ra = 1950$ is 10.5015 and 0.4176 when $(L, M) = (513, 32)$ and 10.5017 and 0.4182 when $(L, M) = (1025, 64)$, respectively. The maximum relative deviation of period and translation are less than 0.002 and 0.13 %, respectively, which confirms the sufficiency of the truncation number $(L, M) = (513, 32)$.

https://doi.org/10.1017/jfm.2012.413 Published online by Cambridge University Press

Class of solution	Condition			Convergence criterion
	Real space	Phase space		
Steady	$\boldsymbol{F}(x,y,t)=\boldsymbol{F}(x,y,0)$	$\phi_{lmn}(\boldsymbol{z}^{(0)},t)=z^{(0)}_{lmn}$	$(^{\forall}t)$	$\displaystyle\int_0^t \left\| \left\{ \frac{\partial \phi_{lmn}(\boldsymbol{z}^{(0)},t')}{\partial t'} \right\} \right\| \mathrm{d}t' < \epsilon$
Travelling wave	$\boldsymbol{F}(x+Ut,y,t)=\boldsymbol{F}(x,y,0)$	$\phi_{lmn}(\boldsymbol{z}^{(0)},t)\mathrm{e}^{\mathrm{i}klUt}=z^{(0)}_{lmn}$	$(^{\forall}t,^{\exists}U)$	$\displaystyle\int_0^t \left\| \left\{ \frac{\partial \phi_{lmn}(\boldsymbol{z}^{(0)},t')\mathrm{e}^{\mathrm{i}klUt'}}{\partial t'} \right\} \right\| \mathrm{d}t' < \epsilon$
Time-periodic	$\boldsymbol{F}(x,y,\tau)=\boldsymbol{F}(x,y,0)$	$\phi_{lmn}(\boldsymbol{z}^{(0)},\tau)=z^{(0)}_{lmn}$	$(^{\exists}\tau)$	$\|\{z^{(0)}_{lmn}-\phi_{lmn}(\boldsymbol{z}^{(0)},\tau)\}\|<\epsilon$
Travelling wave (2Γ-periodic domain)	$\boldsymbol{F}(x,y,2\Gamma/U)=\boldsymbol{F}(x,y,0)$	$\phi_{lmn}(\boldsymbol{z}^{(0)},2\Gamma/U)=z^{(0)}_{lmn}$	$(^{\exists}U)$	$\|\{z^{(0)}_{lmn}-\phi_{lmn}(\boldsymbol{z}^{(0)},2\Gamma/U)\}\|<\epsilon$
Time-periodic and spatially travelling	$\boldsymbol{F}(x+U\tau,y,\tau)=\boldsymbol{F}(x,y,0)$	$\phi_{lmn}(\boldsymbol{z}^{(0)},\tau)\mathrm{e}^{\mathrm{i}klU\tau}=z^{(0)}_{lmn}$	$(^{\exists}U,^{\exists}\tau)$	$\|\{z^{(0)}_{lmn}-\phi_{lmn}(\boldsymbol{z}^{(0)},\tau)\mathrm{e}^{\mathrm{i}klU\tau}\}\|<\epsilon$

TABLE 1. Conditions for a variety of classes of solutions for $\boldsymbol{F}=(\psi,\theta,\eta)$, where U is a phase/group velocity, τ is a period, t is an arbitrary positive time, $\{\phi_{lmn}\}$ is a flow given by the vector field $\boldsymbol{f}$ defined in (3.10), $\boldsymbol{z}^{(0)}$ is the initial value, $\|\{a_{lmn}\}\|=\sqrt{\sum_{l,m,n}a^2_{lmn}}$, and ϵ is a small positive value that determines the convergence criterion where we choose $\epsilon=10^{-8}$.

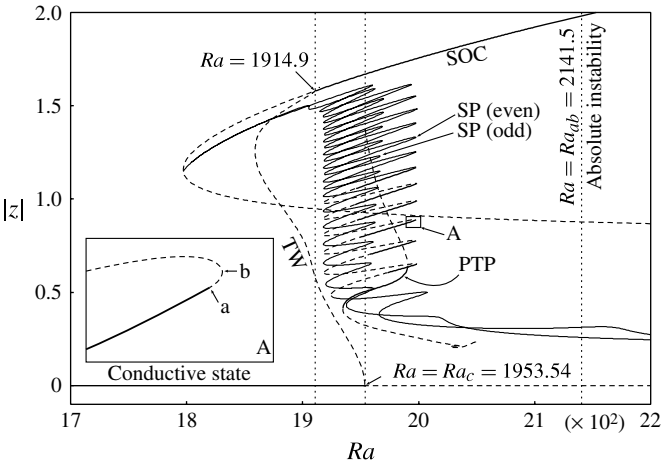

FIGURE 3. Bifurcation structures of various solutions for $\Gamma = 32$. Thick solid lines and thick dashed lines denote stable and unstable solutions, respectively. Although the conductive state $z = 0$ exists for all Ra, it loses stability via subcritical Hopf bifurcation at $Ra = Ra_c = 1953.54$, leading to the unstable TW solution. The TW meets an SOC at $Ra = 1914.9$ and the SOC is stabilized. The wavenumber of the SOC branch corresponds to the critical one around the Hopf point. There are two snake-like branches: even-SP and odd-SP. They are spatially localized and their stability is examined for several branches containing a smaller number of cells (thick lines). Solutions in which stability is not calculated (although the calculation is possible) are indicated by thin solid lines. When we climb up along the snake-like SP branch, two convection cells are added after passing two saddle-node points. The detailed bifurcation structure near A is described schematically in the lower-left inset. It should be noted that stability does not change at saddle-node point b but at point a, slightly before the saddle-node point, because the second or lower-order eigenvalue changes sign at each saddle-node point. In contrast to SPs, PTP solutions do not form snake-like structures but lose and gain stability via saddle-node bifurcation. Note that stable SP and PTP solutions exist outside of the bistable region ($Ra > Ra_c$). Also note that the PTP solution branch does not connect to the SP branch at the upper end of the PTP branch, but the continuation of the branch is difficult because the period of deformation of a PTP becomes very large as $|z|$ increases, which means that the number of convection cells in a PTP is large. Note that the PTP branch ends up with open ends because of the numerical difficulty.

4. Convection patterns and their stability in binary fluid mixture

In this section, we present a variety of classes of solutions, together with their stability, to explain the complex pattern formation in figure 1. The solutions characterized in table 1 and another type of solution characterized by quasi-periodicity are presented in §§ 4.1 and 4.2, respectively.

4.1. *Solutions*

For the solution branches defined in table 1 at $\Gamma = 32$ (figure 3), when Ra is small, only the stable conduction solution $z = 0$ exists. The conductive state loses stability via subcritical Hopf bifurcation at $Ra = Ra_c = 1953.54$ and the unstable travelling-wave (TW) solution emerges. The TW branch meets the SOC solution and the SOC solution is stabilized at $Ra = 1914.9$. Thus, there exists a bistable region between $1914.9 \leqslant Ra \leqslant Ra_c$ where both the conductive state and the SOC are stable.

The instability in the region $Ra > Ra_c$ has been studied by Batiste *et al.* (2006). They divided the region $Ra > Ra_c$ into two parts: one where the conductive state

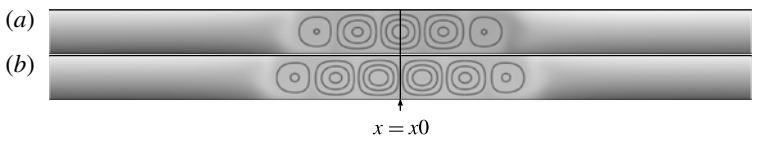

FIGURE 4. Examples of (*a*) odd-SP solution and (*b*) even-SP solution for $Ra = 1950$. Both solutions correspond to the SP with the minimum number of cells. Other numbers of cells are possible in the limit of system size. Note that only part of the domain $16 \leqslant x \leqslant 48$ is shown.

shows convective instability and one where it shows absolute instability (Huerre & Monkewitz 1990). When the state has convective instability (indicated in figure 3: see Appendix for details), a small perturbation becomes a propagating wave packet that grows exponentially in amplitude on the co-moving coordinate. However, in the laboratory frame, the amplitude finally converges to zero at any point.

SP solutions appear as two snake-like branches. They represent localized convection cells: cells are confined to a spatially localized region (convection region) and outside that region, the state is similar to the conductive state (see figure 4). This solution is steady and is classified as the steady solution in table 1. Two branches constructed by SP solutions are termed the even-SP branch and odd-SP branch, depending on the number of convection cells. The two branches can be identified by their symmetry. For the even-SP branch, the symmetry for ψ, θ, η is given by

$$\begin{cases} \psi(x - x_0, y, t) = -\psi(-(x - x_0), y, t), \\ \theta(x - x_0, y, t) = \theta(-(x - x_0), y, t), \\ \eta(x - x_0, y, t) = \eta(-(x - x_0), y, t), \end{cases} \tag{4.1}$$

and for the odd-SP branch, we have

$$\begin{cases} \psi(x - x_0, y, t) = \psi(-(x - x_0), -y, t), \\ \theta(x - x_0, y, t) = -\theta(-(x - x_0), -y, t), \\ \eta(x - x_0, y, t) = -\eta(-(x - x_0), -y, t), \end{cases} \tag{4.2}$$

where x_0 is the centre of the SP (see figure 4).

When we trace each branch from the bottom of the bifurcation diagram, the number of cells increases by two as the branch passes two saddle-node points. The regions where snake-like branches of the even- and odd-SP solutions exist overlap with the bistability region ($1914.9 < Ra < Ra_c$). However, stable SP solutions also exist when $Ra > Ra_c$, that is, where the conductive state is unstable.

We remark that the stability of SP solutions does not change at the saddle-node point, where the sign of the first eigenvalue remains positive, but the sign of the second or lower eigenvalue changes there. The first eigenvalue changes the sign at a point close to the saddle-node point (see the inset of figure 3). A similar bifurcation diagram is obtained for the Swift–Hohenberg equation (Burke & Dawes 2012).

PTP solutions form another branch (figure 3) that, like SP solutions, represents spatially localized patterns consisting of finitely many convection cells – but it is not steady (figure 5). The convection cells are created at one end of the convection region, but at the same time, disappear at the other end of the region. Thus, the PTP solution is achieved by a balance between the creation and destruction of convection cells. Moreover, its envelope propagates at a constant speed (group velocity) in the laboratory frame. If we observe the PTP solution in a frame moving with the group

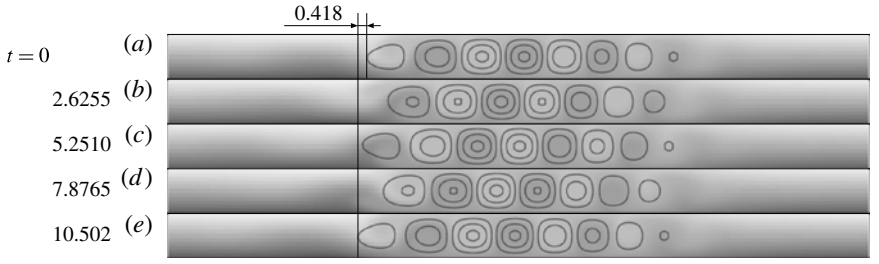

FIGURE 5. PTP solution for $Ra = 1950$. The background colour denotes the concentration field: black is high density, white is low density. Black solid lines denote stream lines. The period τ is 10.502 and the increment of the PTP pattern during a period $U\tau$ is -0.418. Note that only part of the domain $16 \leqslant x \leqslant 48$ is shown. All values are non-dimensionalized.

velocity, the pattern is time-periodic. Therefore, in addition to each component of $z^{(0)}$, obtaining the PTP solution requires two unknowns, the group velocity and the period. It is classified as the time-periodic spatially travelling solution in table 1. The global behaviour of a PTP solution branch, as detailed by Watanabe *et al.* (2010), is less snaky and includes only one stable solution for a given Ra. And in contrast to the SP solution, the PTP solution loses its stability via saddle-node bifurcation (see figure 3). Moreover, the stable PTP solution also exists outside the bistability region, where the conductive state is unstable. These facts are consistent with the experiment conducted by Niemela *et al.* (1990) because they reported that PTPs (LTWs in their notation) also exist above critical Ra and, moreover, are only observed below a certain value.

The origin of bistability can be traced back to the effect of the concentration field. As mentioned earlier, when the separation ratio S is negative, the Soret effect suppresses the onset of convection, which increases the Ra-value of the instability of the conductive state. In contrast, if convective motion already exists, the Soret effect does not play an important role because of mixing, allowing the convection cells to persist for the same Ra-values. Recall that we assume $Le \ll 1$ $(D \ll \kappa)$; thus, concentration diffusion is much slower than that of momentum and temperature and therefore the mass flux is nearly passive. Therefore, once a spatially localized convection region is activated, the non-uniform field is maintained. In terms of the bifurcation diagram, the two states correspond to the bistability. Therefore, we can consider SP solutions as describing a convection region sandwiched between conduction regions. The PTP solution may also be understood similarly; however, the convection region is maintained instead by the birth and death of convection cells.

Although stable SP and PTP branches are detected, as in figure 3 for $\Gamma = 32$, even if the conductive state becomes unstable, a natural question is how they are stabilized from a dynamical point of view. What we observe in our numerics is that small fluctuations grow and travel in the unstable conductive region as wave packets and collide with SPs or PTPs. However, they are not strong enough to destroy them and are instead absorbed by them. This is because the system size ($\Gamma = 32$) is small enough to prevent wave packets from growing sufficiently large to affect the existing structures (Batiste *et al.* 2006). However, if the domain is large enough, such wave packets will grow to form a localized structure, as shown in figure 1. Then the interaction between such structures becomes more complex, and this should be treated in a separate way. We discuss the details of the domain-size effect and interaction between such structures in § 6.

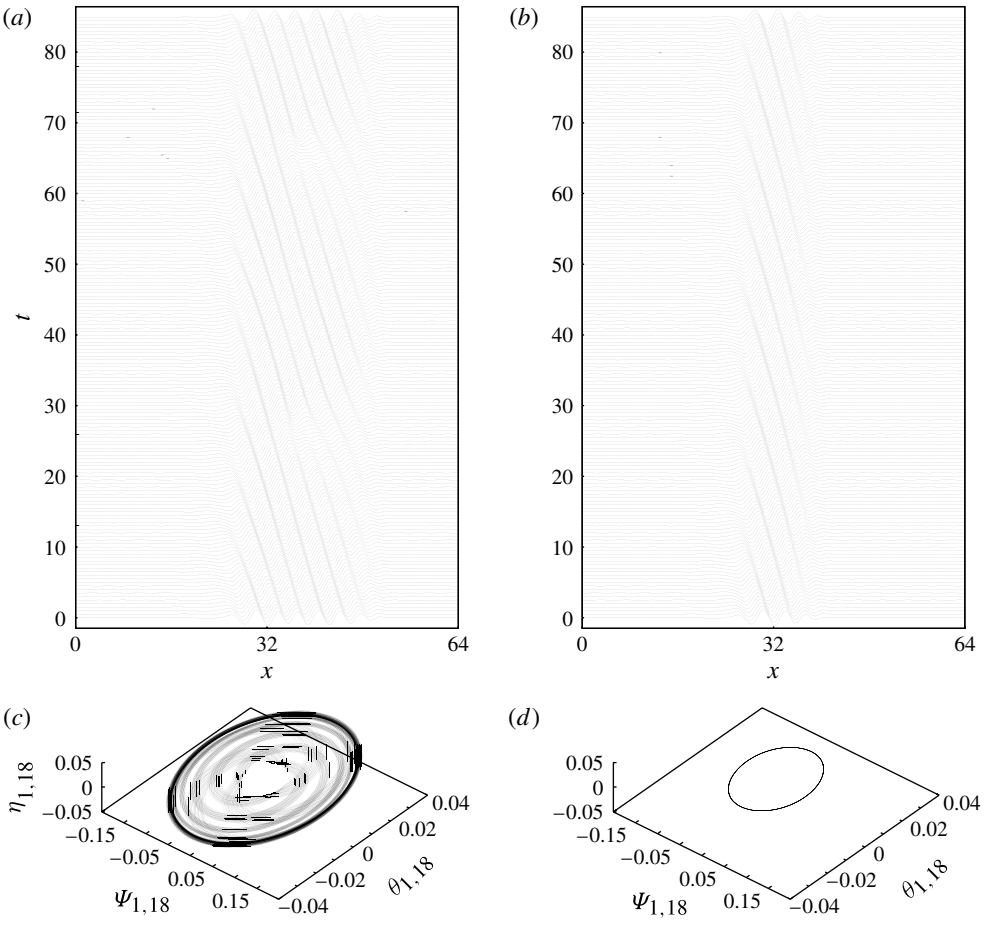

FIGURE 6. (*a,b*) Time evolution plots of $\psi(x, 0, t)$ and (*c,d*) phase plots of (*a,c*) PTP cousin and (*b,d*) PTP. Note that in both, $\psi(x, 0, t)$ is observed in the frame of reference moving with the group velocity of the PTP solution. Although the shape of the pulse is different, the group velocity is almost the same. The PTP solution is time-periodic whereas the PTP cousin is quasi-periodic.

4.2. *PTP cousin*

We find another PTP-like pulse as shown in figure 6; however, it is not detected as a bifurcation branch. We designate it as the 'PTP cousin' because the group velocity is almost the same as that of the PTP. It is difficult to specify the position of the PTP cousin because it is not time-periodic; however, as shown in figure 1, the slope of the track of two PTP cousins (e and f) is almost the same as that of the PTP. Thus, we could estimate the group velocity of the PTP cousin as a long time-averaged velocity.

PTP cousins are obtained both by an asymptotic state of generic initial conditions (see e, f in figure 1*b*) and as a result of collisions (see figure 10). We extracted PTP cousins from these results and calculated their time evolution in a smaller domain ($\Gamma = 32$). Calculations for larger truncation numbers ($M = 36$ and $L \approx 32\Gamma$, which is about twice the size of general calculations) were also performed. These examinations confirmed that the PTP cousin is neither an artifact of numerical error nor the result of a size effect.

Indeed, we have not succeeded in obtaining a PTP cousin as a solution branch because it seems to be quasi-periodic, as shown in figure 6(*c*). Thus, the conditions for such a solution are not expressed in the form shown in table 1.

A similar structure is reported in doubly diffusive convection; see Beaume, Bergeon & Knobloch (2011), the leftmost panel of figure 14.

5. Pattern formation in a large domain

In this section, asymptotic behaviour in a large periodic domain ($\Gamma = 500$) is examined. We have chosen $Ra = 1960$, at which the conductive state is convectively unstable but SP and PTP solutions exist when $\Gamma = 32$ (figure 3).

Figure 1(*a*) shows a time evolution started from a pointwise initial disturbance at $x = 500$ with a pair of small convection cells having the symmetry described by (4.1). The amplitude of the disturbance is about ten times smaller than that of an SOC. At first, the initial disturbance splits into two wave packets propagating in opposite directions, B1 and B2. Initially, the amplitudes of the wave packets are sufficiently small for linearity to hold; thus, their collisions appear to be simply superpositions of the wave packets with no significant interactions. As the amplitude of the wave packet grows, however, it forms a travelling pulse similar to the PTP solution (§ 3) and also spreading disturbances over a wide range ($t \approx 1000$). Some of these disturbances grow to form a localized structure that is wider than the PTP or PTP cousin.

At C1 and C2 ($t \approx 4000$), a collision between a travelling pulse and the localized structure is observed. As a result, a single travelling pulse survives. The symmetry of the distribution of the large-scale structure is broken at $t \approx 5000$ by the creation of other coherent structures (D).

After the collision at E, all of the large-scale structure moves in the left direction. In the period $6250 < t < 6750$, only two travelling pulses exist. Because the interval between pulses is wide enough, perturbations in the interval can grow to form other localized structures (F). Such localized structures experience many interactions, and finally produce an array of four travelling pulses, all of which are similar to the PTP. The distribution of the pulses is not uniform, but is maintained for a long time (over 10 000 units of time).

Besides strong interactions (collisions), there are interactions between travelling pulses and wave packets, termed as ‘mild interactions’. Because the velocity of the wave packet is larger than the group velocities of the travelling pulses, the wave packet can catch up with the pulse. When the wave packet has a small amplitude, it is absorbed by the travelling pulse; the velocity and the shape of the travelling pulse do not change significantly. When the amplitude is slightly larger, however, the shape of the pulse is temporally deformed, although it finally recovers its original shape. Nevertheless, due to the interaction, the position is shifted (*a–d*). The birth of a new pulse, as at D and F, occurs again at G ($t \approx 25750$, $x \approx 500$), because the interval between PTPs is large enough to allow the growth of wave-packet disturbances.

Compared with the time evolution from a random disturbance with an amplitude 10^{-10} times smaller than that of an SOC, as in figure 1(*b*), we see that although the details are different, the spatio-temporal pattern consists of processes similar to those in figure 1(*a*). First, we observe the growth of a disturbance into a wave packet. Second, after the amplitude of this wave packet is large enough, a travelling wave is generated. The shape is similar to the PTP or PTP cousin, but we observe another localized structure wider than either the PTP or PTP cousin (H), although the structure is not stable. Finally, it converges to a pulse similar to the PTP (or PTP cousin).

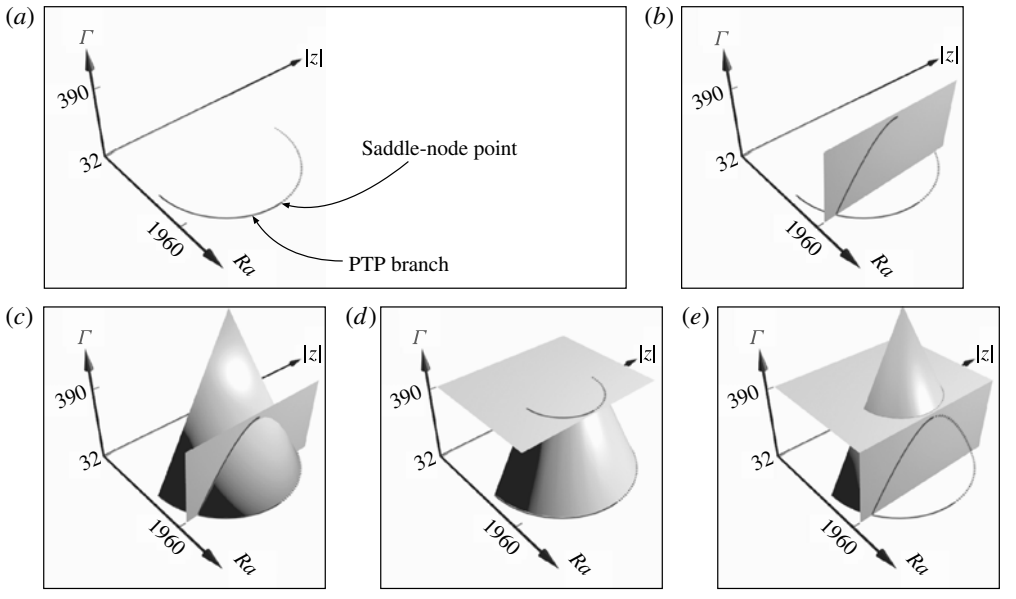

FIGURE 7. (*a*) Detection of the maximum aspect ratio Γ_M. (*b*) A stable PTP bifurcation branch on the $\Gamma = 32$ plane is extended on the Γ–$|z|$ plane at $Ra = 1960$. (*c*) The result implies the existence of an ice-cream-cone-like bifurcation surface. (*d*) A saddle-node point is expected to exist on the Ra–$|z|$ plane at $\Gamma = 390$. (*e*) A saddle-node point also appears on the Γ–$|z|$ plane at $Ra = 1960$.

From these simulations, we propose a scenario for the pattern formation process in the large domain as follows. (i) A disturbance in the background state (similar to the conductive state) grows into a wave packet due to the convective instability. (ii) If the region for the background is large enough, the wave packet forms a coherent structure similar to the PTP, the PTP cousin (travelling pulse), and localized travelling pulses with larger width, a 'fat' PTP. However, the fat PTP becomes thinner as it propagates. In the asymptotic state, we only observe the PTP or the PTP cousin. (iii) The interaction between a travelling pulse and a wave packet results in a single travelling pulse. (iv) Interactions between two travelling pulses also result in a single travelling pulse. (v) If SP solutions exist, those pulses do not survive because they eventually become PTP(s) as a result of collisions (see § 6.2 and figure 9). In the following section, we focus on the elementary processes constituting pattern formation.

6. Elementary process of pattern formation

6.1. *Critical aspect ratio for PTP*

As shown in figure 3, a single PTP solution is stable at $Ra = 1960$ for $\Gamma = 32$, but it becomes unstable when $\Gamma = 500$. Therefore, for a single PTP, there is a range of aspect ratios where the PTP solution is stable. Here, we obtain the range $\Gamma_m < \Gamma < \Gamma_M$ by estimating the values of Γ_M and Γ_m at $Ra = 1960$, where Γ_M and Γ_m are the largest and the smallest aspect ratio for a single PTP, respectively.

First, we study the largest aspect ratio Γ_M. Since it is difficult to calculate a PTP solution for large Γ, time-evolution calculations are performed to find stable PTPs, as shown schematically in figure 7. We followed a stable PTP branch on the Γ–$|z|$ plane

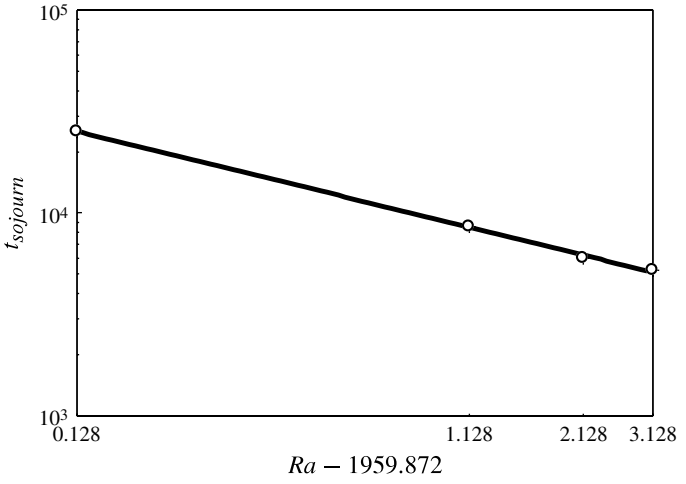

FIGURE 8. Sojourn time of a solitary PTP for $\Gamma = 390$ versus $Ra - 1959.872$. Outline circles denote sojourn times obtained by numerical simulation, which are fitted by the thick solid line $t_{sojourn} = 9031.74 \times (Ra - 1959.872)^{-1/2}$.

(recall (3.11) for the definition of z) from $\Gamma = 32$ by continuation (figure 7*b*) and found that it disappears around $\Gamma = 390$. We have at least two explanations for why the stable PTP branch disappears: one is that the single PTP solution at $\Gamma = 390$ still exists but is unstable; the other is that the single PTP solution disappears. If the latter picture is valid, the solution surface of the PTP in Ra–Γ–$|z|$ space has a conical shape near the region determined by $\Gamma = 390$, $Ra = 1960$ (figure 7*c*). Thus, if we cut the cone at $\Gamma = 390$, there is a saddle-node point around $Ra = 1960$ on the Ra–$|z|$ plane at $\Gamma = 390$ (figure 7*d*). To confirm this expected saddle-node point, time-evolution calculations for $Ra = 1960$, 1961, 1962 and 1963 were performed at $\Gamma = 390$ and the sojourn time near a single PTP was examined. A plural-PTP state is achieved via a typical transition process: (i) convective wave-packet disturbances, which propagate in the same direction as that of the PTP, grow and collide with the PTP from behind it, but many are absorbed by the PTP in an early stage; (ii) the PTP is gradually modulated, and the PTP itself emanates new seeds of wave-packet disturbances (recall that the domain is periodic); (iii) some disturbances grow sufficiently to break down the PTP; (iv) the PTP breaks and almost disappears; (v) two or more PTPs appear. Therefore, the phase-space vector z passes through near the conductive state before it goes to the plural-PTP state and thus $|z|$ experiences a local minimum between the initial and the final state. This local minimum is detected as the end of the sojourn time.

As shown in figure 8, the sojourn time $t_{sojourn}$ obeys the function of Ra as

$$t_{sojourn} = 9031.74 \times (Ra - 1959.872)^{-1/2}. \tag{6.1}$$

The $-1/2$ law supports the existence of a saddle-node point at $Ra = 1959.872$. Then, there also appears a saddle-node point at $\Gamma \approx 390$ if we project the conical solution surface onto the plane $Ra = 1960$ (figure 7*e*). Therefore, we detect Γ_M as $\Gamma_M \approx 390$, and there exists no single PTP solution beyond Γ_M.

For Γ_m, we calculated successive time evolutions of a single PTP by decreasing Γ gradually. The initial condition was set up by removing the conductive state just

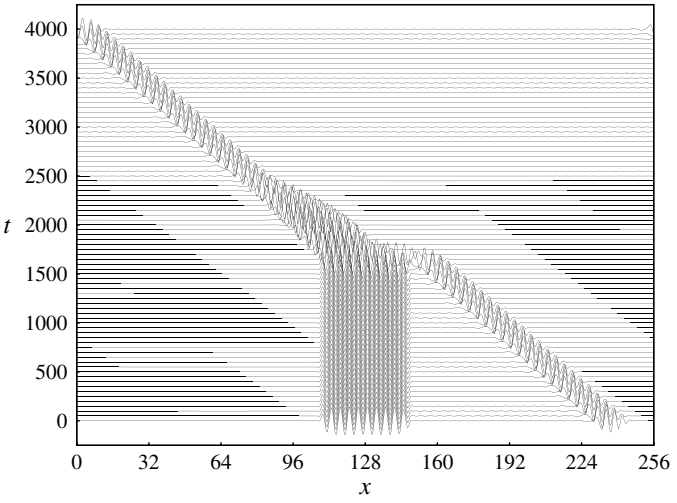

FIGURE 9. Collision between 20-cell SP (centre at $t = 0$) and leftward-moving PTP (right end at $t = 0$). $\psi(x, 0, t)$ is shown. The SP cannot survive the collision.

behind the PTP obtained by simulation at a slightly larger value of Γ. As a result we found that Γ_m is in the range [9.658, 9.659].

Note that if a plural-PTP state is achieved, the system can approximately be regarded as small independent fragments, where the distance of each fragment does not exceed Γ_M and is larger than Γ_m. Therefore, we estimate the number of PTPs in a domain Γ, N as

$$\left[\frac{\Gamma}{\Gamma_M}\right] < N < \left[\frac{\Gamma}{\Gamma_m}\right], \tag{6.2}$$

which is $2 \leqslant N \leqslant 51$ for $\Gamma = 500$, where $[\cdot]$ is the Gauss symbol. The numbers of PTPs and PTP cousins in the two cases in figure 1 were four and five, which is within the range of this estimation. Note that plural PTPs can coexist if $\Gamma \geqslant 2\Gamma_m$, as has been observed in experiment (Niemela *et al.* 1990).

The existence of a critical domain size suggests that large domain sizes should be considered separately. In particular, a single PTP solution outside the bistable region does not exist for large domain size because the PTP solution vanishes through the saddle-node bifurcation. Therefore it is conjectured that bifurcation branches of PTPs in figure 3 may change their shape according to the aspect ratio because their saddle-node points shift to the left (lower-Ra) direction for larger Γ, and they might eventually approach or enter the bistable region when $\Gamma \to \infty$.

6.2. *SP–PTP collision*

There are several stable SP solutions at $Ra = 1960$ in the bifurcation diagram shown in figure 3, however no SP appears in the asymptotic state in figure 1. To check the robustness of the SP solutions, we simulated collisions between PTPs and several SP solutions characterized by the number of active cells (from 6 to 20 cells) at $\Gamma = 128$. In all cases, SP–PTP collisions result in a single PTP; a typical collision (20-cell SP and PTP) is shown in figure 9. Thus, even if an SP exists, it will be destroyed by a collision with a PTP.

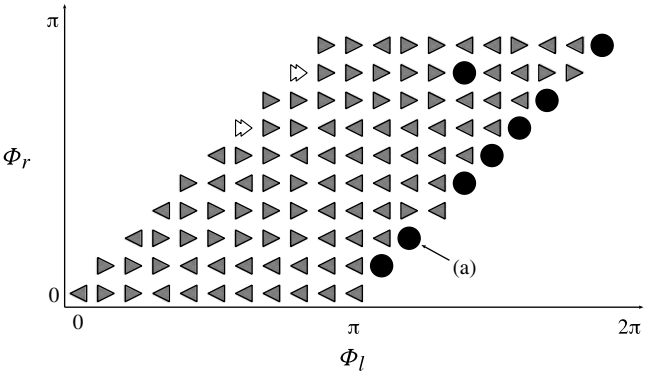

FIGURE 10. Phase dependence of PTP–PTP collisions: •, SOC; ◁, leftward-moving PTP; ▷, rightward-moving PTP; ▷, rightward-moving PTP cousin.

6.3. *PTP–PTP collision*

In the time evolutions, we often observed a collision between travelling pulses. In all cases, the final result was a single PTP. Here we study the collision processes in detail. It was reported that the collision results depend sensitively on the Rayleigh number even if the initial conditions are the same (Toyabe 2009), although the initial conditions were constructed by travelling pulses obtained as the asymptotic state of the time evolution. As is mentioned in § 4.1, the PTP solution is a time-periodic spatially travelling solution; thus, the state has a phase when we observe the PTP solution in the moving frame. Thus, for a complete analysis of the collision, we need to control the phase for both leftward- and rightward-propagating PTPs (Watanabe *et al.* 2010).

We define the phase of the solution at $t = t_0$ by $\Phi = 2\pi \times t_0/\tau \pmod{2\pi}$, where τ is the period of the solution. Then we prepare $P_r(\Phi_r)$ and $P_l(\Phi_l)$, the rightward- and leftward-moving PTPs, where Φ_r and Φ_l are the initial phases, respectively. The initial conditions for the collision are constructed by positioning P_r and P_l with an interval of 64. The system size Γ is 64 (spatial period is 128).

We show the collision results for all the possible combinations of (Φ_r, Φ_l) in figure 10, with the symmetry of the PTP solution as

$$\begin{cases} -\psi(x - U\tau/2, -y, 0) = \psi(x, y, \tau/2), \\ -\theta(x - U\tau/2, -y, 0) = \theta(x, y, \tau/2), \\ -\eta(x - U\tau/2, -y, 0) = \eta(x, y, \tau/2), \end{cases} \tag{6.3}$$

and invariance under the transformation $x \to -x$.

Figure 10 shows that the results are either a single PTP, a PTP cousin, or an SOC. The interaction processes for these results are categorized by the phase difference $\Phi_d = |\Phi_l - \Phi_r|$. They can be classified into three categories as shown in figure 11. (I) In most cases, mainly $0 < \Phi_d < \pi$, only one PTP is selected immediately after the collision (figure 11*a*). (II) If $\Phi_d = 0$, where the initial conditions have mirror symmetry, two PTPs appear to annihilate each other after the collision, but a new pair of counter-propagating PTPs is generated again. These PTPs undergo a second collision, producing either a rightward- or leftward-moving PTP. During the collision process, the mirror symmetry is lost due to the accumulation of numerical error. As a result, the phase difference at the second collision is not zero, which leads to a single PTP (figure 11*b*). (III) If $\Phi_d = \pi$, once they fuse into an 11-cell SP, both fronts of the

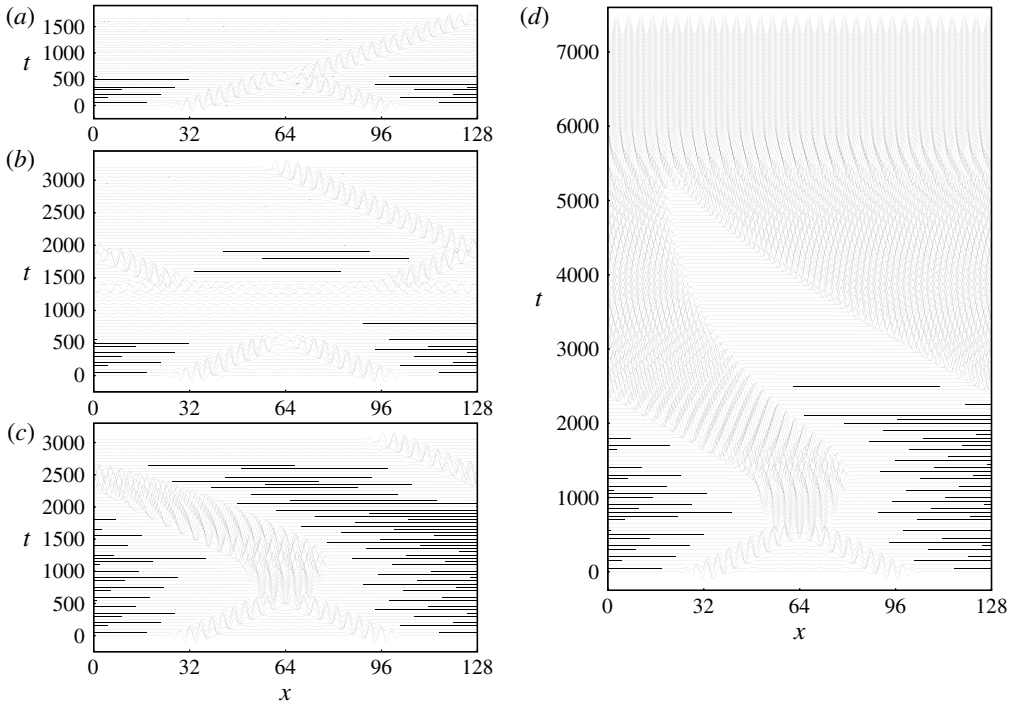

FIGURE 11. Four typical transition processes ($\psi(x, 0, t)$ is shown). (*a*) Immediate convergence to a single PTP. (*b*) Collision once results in annihilation; two counter-propagating PTPs emerge again; collision occurs again, and they merge into a single PTP. (*c*) Collision once results in an SP but it starts moving and converges into a PTP. (*d*) Collision once results in an SP; both its fronts stretch out while breaking the initial symmetry; then it starts moving and finally converges into an SOC.

SP stretch out with an increasing number of convection cells after losing the initial symmetry (4.2). Then it starts moving. It converges to a PTP if the symmetry breaking occurs before the increase in the number of cells (figure 11*c*). By contrast, it converges to an SOC if the increase in the number of cells occurs earlier (figure 11*d*).

As classified above, the collision seldom results in an SOC. The basin area of an SOC is estimated by the probability of SOC occurring, which is indicated by the filled circles in figure 10. Similar numerical experiments for phase differences around $\Phi_d = \pi$ revealed that SOCs exist when $\Phi_d \leqslant 2\pi/2300$ in all seven cases except (a) in figure 10 and when $\Phi_d \leqslant 6\pi/2300$ for case (a). The area of the basin is less than 0.1 % in all representative initial conditions. The results show that the flow converges to PTPs in almost all cases and only rare initial conditions result in an SOC.

In sum, except for rare cases where an SOC appears, a sufficiently large conductive region for $Ra = 1960$, where a trivial state is convectively unstable, results in PTPs and PTP cousins that move in the same direction and are arranged in non-uniform intervals.

7. Conclusion

We study spontaneous pattern formation and its asymptotic behaviour in binary fluid flow driven by a temperature gradient. We succeeded in obtaining time-periodic travelling pulses (PTPs) globally in parameter space as numerical solutions which

satisfy appropriate mathematical conditions including unstable ones, and clarified their important role in the characterization of asymptotic behaviour in a large but finite domain (see also Watanabe *et al.* 2010). In contrast to a pure fluid, localized patterns such as steady pulses (SPs) and PTPs appear, in addition to the conventional Rayleigh–Bénard convection pattern (SOC).

Despite the long history of studying PTPs via experiments (Heinrichs *et al.* 1987; Kolodner *et al.* 1988; Niemela *et al.* 1990; Kolodner 1991), the numerical approach (Barten *et al.* 1991, 1995; Ning *et al.* 1996; Jung *et al.* 2004; Toyabe 2009), and the theoretical model based on the amplitude equations (Thual & Fauve 1988), detailed analysis of the pattern formation process had not been possible because the PTP is a time-periodic travelling solution, and the state is determined not only by the position of the envelope but also by the phase of the internal convection structure. Although Iima & Nishiura (2009) investigated the collision process of two counter-propagating PTPs by extended complex Ginzburg–Landau equations and their results agree with those of experiment qualitatively, they pointed out the importance of the internal structure of PTPs, which cannot be resolved by the amplitude equations. A numerical solution satisfying the mathematical conditions has made it possible to analyse the interaction process in detail (Watanabe *et al.* 2010).

We obtained the global bifurcation diagram for the aspect ratio $\Gamma = 32$ (figure 3). A stable PTP solution as well as a stable SP solution exists outside the bistable region, where the conductive state is linearly unstable. Similar phenomena were observed by Niemela *et al.* (1990), where the convective instability was suggested. This is counter-intuitive because a small perturbation added to the conductive state may grow and destroy these localized patterns. Therefore, such peculiar solutions are considered to be the result of the finiteness of the domain. This naturally leads to the following question: What happens in a finitely large domain if the conductive state is linearly unstable?

To examine this question, we performed time-evolution calculations with generic initial conditions in a large periodic domain ($\Gamma = 500$), much larger than that used for the bifurcation diagram ($\Gamma = 32$). The Rayleigh number Ra was set to be 1960, where the conductive state is linearly unstable. Figure 1 shows typical results of these calculations. Interestingly, no single SP or PTP state is realized in spite of the fact that they are stable when $\Gamma = 32$. Instead, an array of PTPs and PTP cousins moving in the same direction and arranged at non-uniform intervals are obtained. This implies the existence of a critical aspect ratio Γ_M above which a single and stable PTP cannot be observed.

Then the next question addressed is the following: How does the stable PTP branch disappear at Γ_M? To elucidate the nature of Γ_M, the stable PTP branch at $Ra = 1960$ was extended to larger Γ. We found that the single PTP solution disappears around $\Gamma = 390$ (figure 7*b*); $\Gamma_M \approx 390$ for $Ra = 1960$. We confirmed that the critical Ra of the saddle-node point for $\Gamma = 390$ ($Ra = 1959.872$) is much smaller than that for $\Gamma = 32$ ($Ra = 1990.61$). In figure 1, because $\Gamma_M < \Gamma = 500$, the asymptotic states are expected to be patterns consisting of at least two PTPs.

In terms of pattern formation in a large domain, we have another question: Why was no SP observed? To clarify this point, the collision process between SP and PTP was simulated, which showed that SPs are overwhelmed by PTPs. Thus, the transient of the asymptotic behaviour results in interactions between PTPs. Therefore, to understand the asymptotic behaviour in a large domain, interactions between PTPs are important.

Hence PTP–PTP collisions were examined, as in figure 10, which showed that, in most cases, a single PTP is generated as the result of a collision. A PTP cousin, a

PTP-like moving pulse as shown in figure 6, is sometimes also generated. However, it can be regarded as having the same structure as a PTP in this context because the group velocity is almost the same. Thus, a PTP and PTP cousin that propagate in the same direction do not collide: both of them persist. Although an SOC is generated in a few cases, we do not need to take it into account because the basin area of SOCs is less than 0.1 %. In addition, the realization of SOCs strongly depends on the system size, as shown in figure 11(*d*) and figure 1 (H), because a 'fat' PTP gradually becomes a PTP or PTP cousin (H in figure 1) as long as the two fronts of the envelope do not meet each other (figure 11*d*).

The results of these analyses confirm the asymptotic behaviour in a large domain as shown in figure 1: an array of unequally spaced PTPs moving in the same direction.

In these analyses, the size of the system Γ is an essential factor because a linearly unstable conductive state is convectively unstable, as shown in figure 3. In a convectively unstable state, the asymptotic state depends on whether wave-packet disturbances can grow sufficiently large to influence the results. If Γ is small, they are absorbed by the existing pulse and then a single pulse is stable. But if Γ is large enough, the disturbances grow sufficiently to break the existing pulse; a single pulse in the system is no longer stable, and other pulses appear between them and collisions occur. Thus, system size can be divided into three categories:

(i) small (a solitary PTP exists);

(ii) large enough but finite (a solitary PTP cannot exist);

(iii) infinite.

The difference between small (i) and finitely large (ii) is distinguished by the critical aspect ratio $\Gamma_M(Ra)$. A single PTP is possible when Γ is smaller than $\Gamma_M(Ra)$ but impossible when it exceeds $\Gamma_M(Ra)$ and, instead, an array of PTPs or PTP cousins is realized after complicated transition processes. For the infinite system (iii), the asymptotic behaviour might be very different from (ii). Some implications for $\Gamma \to \infty$ were also obtained via the analysis to determine Γ_M, because the critical Ra of the saddle-node point of the PTP solution seems to decrease. These observations suggest that the saddle-node point approaches or enters the bistable region when Γ approaches infinity.

Spontaneous pattern generation and the interactions among these patterns have been studied in many other systems, for example, barchan dunes (Katsuki *et al.* 2005) and reaction–diffusion systems (Nishiura, Teramoto & Ueda 2003*a*; Nishiura *et al.* 2003*b*; Teramoto *et al.* 2004). These studies are useful for understanding pattern formation, in general. Among them, an example of travelling spots in a two-dimensional reaction–diffusion system (Nishiura *et al.* 2005) resembles the present case in terms of the asymptotic behaviour. In this system, when a single spot is given at $t = 0$, self-replication occurs again and again and the newly born spots travel, collide, and eventually form a marching, spatially periodic pattern with the same velocity. The number of spots in a system is determined by the system size. However, the essential difference between them is the instability property. For travelling spots, self-replication occurs through the instability of each spot itself and the background homogeneous state is stable. By contrast, in the present system, the PTP itself is stable and the background conductive state is unstable.

We remark that further investigation is needed for the SP solution. The first problem is how the stability interval or the saddle-node point changes when the domain size becomes large. A preliminary result suggests that the saddle-node point of the SP branch does not change significantly like the PTP case when $\Gamma = 500$, but some SP solutions that are stable when $\Gamma = 32$ become unstable. Because the difference

between the tail part of the SP solution and the conductive state becomes unlimitedly small in the limit $\Gamma \to \infty$, it is expected that the SP solution becomes unstable or vanishes in the limit $\Gamma \to \infty$ when the conductive state is unstable. The second problem is the role of the SP as the separator in a collision process. We sometimes observe unstable SP solutions as transient states in the PTP–PTP collision (Toyabe 2009); the SP looks unstable but its unstable manifold controls the final states after collision. Clearly, the detailed mathematical structure for SP solutions is useful and it should be further investigated. We will report the details elsewhere.

In sum, remarkably unique pattern formation phenomena exist in the present case; the differences from phenomena in other systems must be stressed. In many systems, localized patterns are generated in a bistable region, or, even if only one state is stable, the background state is stable. However, in the present system, the situation is the opposite because the background conductive state is unstable and is the origin of the pattern generation. However, many interesting properties of binary fluid convection remain to be explored in future work, for example, collisions between a PTP and PTP cousin or between two PTP cousins, the stability of SP solutions, and the stabilization mechanism for the unstable conductive state through the existence of pulses. Here, it should be stressed again that the present system is very different from other systems because patterns are generated via interactions between the instability and stabilization of the background state, which leads to a general framework, that is, *stable patterns in an unstable field*. More detailed analysis for binary fluid convection is expected to lead us to a complete understanding of such a general framework.

Acknowledgements

This study was partially supported by a Grant-in-Aid for Scientific Research (KAKENHI; No. 21340019) and by the Core Research for Evolutional Science and Technology (CREST; No. PJ74100011).

Appendix. Convective instability

In this section, the stability of the conductive state above and near the Hopf point is examined.

Adding perturbations $(\psi, \theta, \eta) = (\psi(y), \theta(y), \eta(y))\mathrm{e}^{\lambda t + \nu x}$ to the conduction solution $\psi = \theta = \eta = 0$ and linearizing (2.5)–(2.7) around the trivial solution, a generalized eigenvalue problem is obtained as follows:

$$\lambda \begin{pmatrix} \Psi_m'' + \nu^2 \Psi_m & 0 & 0 \\ 0 & \Theta_m & 0 \\ 0 & 0 & H_m \end{pmatrix} \begin{pmatrix} \psi_l \\ \theta_l \\ \eta_l \end{pmatrix} = \begin{pmatrix} \sigma(\Psi_m^{\mathrm{iv}} + 2\nu^2 \Psi_m'' + \nu^4 \Psi_m) & -\dfrac{\sigma Ra(1+S)\nu}{16}\Theta_m & \dfrac{\sigma RaS\nu}{16} H_m \\ -\nu \Psi_m & \Theta_m'' + \nu^2 \Theta_m & 0 \\ 0 & \Theta_m'' + \nu^2 \Theta_m & Le(H_m'' + \nu^2 H_m) \end{pmatrix} \times \begin{pmatrix} \psi_l \\ \theta_l \\ \eta_l \end{pmatrix}. \tag{A 1}$$

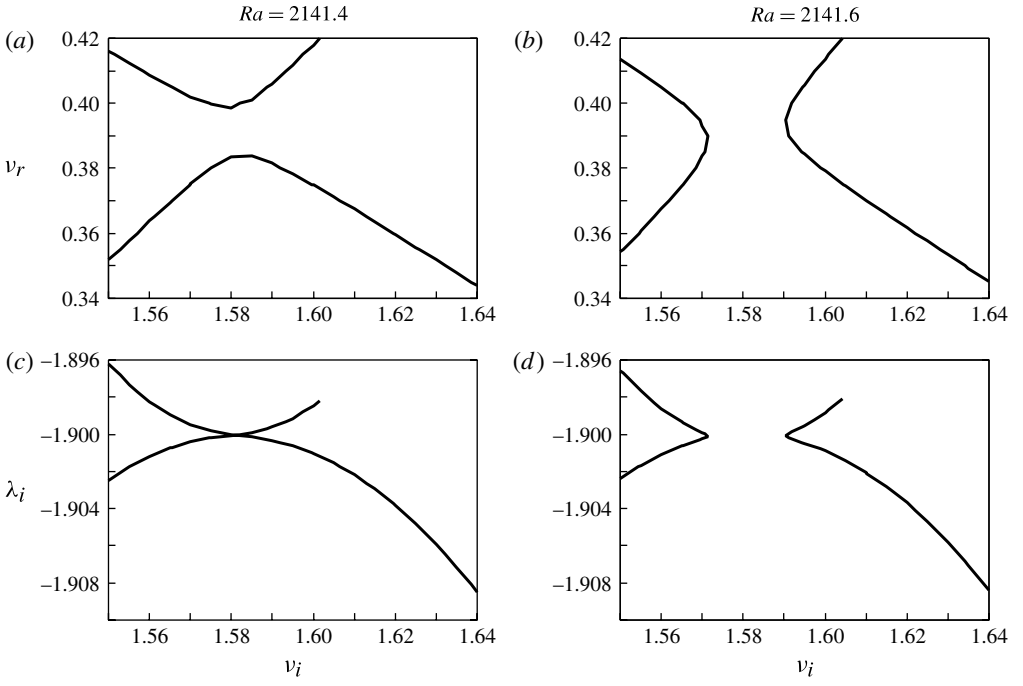

FIGURE 12. Projection of the set of points $A := \{\lambda_r, \lambda_i, \nu_r, \nu_i \mid \lambda_r = 0, \lambda = \lambda(\nu)\}$ onto (a,b) the ν-plane and (c,d) the (ν_i, λ_i)-plane: (a,c) $Ra = 2141.4$; (b,d) $Ra = 2141.6$.

The above equation gives a dispersion relation $\lambda = \lambda(\nu)$. Here λ and ν are written as $\lambda = \lambda_r + \mathrm{i}\lambda_i$ and $\nu = \nu_r + \mathrm{i}\nu_i$, respectively, for the sake of simplicity, where λ_r, λ_i, ν_r, and ν_i are real numbers.

Assume that there exists a complex wavenumber ν_0 such that the corresponding group velocity is zero:

$$\left.\frac{\partial \lambda}{\partial \nu}\right|_{\nu=\nu_0} = 0. \tag{A 2}$$

The system is convectively unstable if the linear amplification rate $\lambda_{r0} := \mathrm{Re}[\lambda(\nu_0)]$ corresponding to ν_0 is negative, because any perturbations are propagated even if they grow. However, the system is absolutely unstable if λ_{r0} is positive because zero-group-velocity perturbations are amplified; that is, there exists a perturbation that grows at a fixed point. The turning point to absolute instability is detected by setting the condition that the eigenvalue $\lambda(\nu)$ has a double root at the threshold of absolute instability (Huerre & Monkewitz 1990), as conducted by Batiste *et al.* (2006). The isoline for $\lambda_r = 0$ is reconnected between $Ra = 2141.4$ and $Ra = 2141.6$, as shown in figure 12. Figures 12(*a*) and 12(*b*) show that there is a saddle-node point around the point $\nu_0 = 0.39 + 1.58\mathrm{i}$ and the linear amplification rate corresponding to the point λ_{r0} changes sign between $Ra = 2141.4$ and $Ra = 2141.6$. Figures 12(*c*) and 12(*d*) show that there exists a cusp point on the algebraic singular point.

Therefore, it is obvious that the critical value for the absolute instability is $Ra \approx 2141.5$ and is far larger than in the Ra region where pulse solutions exist.

Note that figure 1 displays the growth and propagation of packet disturbances. A point disturbance added at point A at $t = 0$ reaches points B1 and B2 at $t = 250$.

REFERENCES

BARTEN, W., LÜCKE, M. & KAMPS, M. 1991 Localized traveling-wave convection in binary-fluid mixtures. *Phys. Rev. Lett.* **66**, 2621–2624.

BARTEN, W., LÜCKE, M., KAMPS, M. & SCHMITZ, R. 1995 Convection in binary fluid mixtures. Part 2. Localized traveling waves. *Phys. Rev.* E **51**, 5662–5680.

BATISTE, O., KNOBLOCH, E., ALONSO, A. & MERCADER, I. 2006 Spatially localized binary-fluid convection. *J. Fluid Mech.* **560**, 149–158.

BEAUME, C., BERGEON, A. & KNOBLOCH, E. 2011 Homoclinic snaking of localized states in doubly diffusive convection. *Phys. Fluids* **23**, 093102.

BECK, M., KNOBLOCH, J., LLOYD, D. J. B., SANDSTEDE, B. & WAGENKNECHT, T. 2009 Snakes, ladders, and isolas of localized patterns. *SIAM J. Math. Anal* **41**, 936–972.

BURKE, J. & DAWES, J. H. P. 2012 Localized states in an extended Swift–Hohenberg equation. *SIAM J. Appl. Dyn. Syst.* **11**, 261–284.

BURKE, J. & KNOBLOCH, E. 2006 Localized states in the generalized Swift–Hohenberg equation. *Phys. Rev.* E **73**, 056211.

BURKE, J. & KNOBLOCH, E. 2007 Homoclinic snaking: structure and stability. *Chaos* **17**, 037102.

BUSSE, F. H. 1964 The stability of finite amplitude cellular convection and its relation to an extremum principle. *J. Fluid Mech.* **30**, 625–649.

CHAPMAN, S. J. & KOZYREFF, G. 2009 Exponential asymptotics of localised patterns and snaking bifurcation diagrams. *Physica* D **238**, 319–354.

CROSS, M. C. 1986 Traveling and standing waves in binary-fluid convection in finite geometries. *Phys. Rev. Lett.* **23**, 2935–2938.

HEINRICHS, R., AHLERS, G. & CANNELL, D. S. 1987 Traveling waves and spatial variation in the convection of a binary mixture. *Phys. Rev.* A **35**, 2761–2764.

HOUGHTON, S. M. & KNOBLOCH, E. 2011 Swift–Hohenberg equation with broken cubic–quintic nonlinearity. *Phys. Rev.* E **84**, 016204.

HUERRE, P. & MONKEWITZ, P. A. 1990 Local and global instabilities in spatially developing flows. *Annu. Rev. Fluid Mech.* **22**, 473–537.

IIMA, M. & NISHIURA, Y. 2009 Unstable periodic solution controlling collision of localized convection cells in binary fluid mixture. *Physica* D **238**, 449–460.

JUNG, D., MATURA, P. & LÜCKE, M. 2004 Oscillatory convection in binary mixtures: thermodiffusion, solutal buoyancy, and advection. *Eur. Phys. J.* E **15**, 293–304.

KATSUKI, A., NISHIMORI, H., ENDO, N. & TANIGUCHI, K. 2005 Collision dynamics of two barchan dunes simulated using a simple model. *J. Phys. Soc. Japan* **74**, 538–541.

KOLODNER, P. 1991 Collisions between pulses of traveling-wave convection. *Phys. Rev.* A **44**, 6466–6479.

KOLODNER, P., BENSIMON, D. & SURKO, C. M. 1988 Traveling-wave convection in an annulus. *Phys. Rev. Lett.* **60**, 1723–1726.

MERCADER, I., BATISTE, O., ALONSO, A. & KNOBLOCH, E. 2011 Dissipative solutions in binary fluid convection. *Disc. Cont. Dyn. Sys.* S **4**, 1213–1225.

NIEMELA, J. J., AHLERS, G. & CANNELL, D. S. 1990 Localized traveling-wave states in binary-fluid convection. *Phys. Rev. Lett.* **64**, 1365–1368.

NING, L., HARADA, Y. & YAHATA, H. 1996 Localized traveling waves in binary fluid convection. *Prog. Theor. Phys.* **96**, 669.

NISHIURA, Y., TERAMOTO, T. & UEDA, K. 2003*a* Scattering and separators in dissipative systems. *Phys. Rev.* E **67**, 056210.

NISHIURA, Y., TERAMOTO, T. & UERA, K. 2003*b* Dynamic transitions through scattors in dissipative systems. *Chaos* **13**, 962–972.

NISHIURA, Y., TERAMOTO, T. & UEDA, K. 2005 Scattering of traveling spots in dissipative system. *Chaos* **15**, 047509.

PLATTEN, J. K. 2006 The Soret effect: a review of recent experimental results. *J. Appl. Mech.* **73**, 5–15.

PLATTEN, J. K. & LEGROS, J. C. 1984 *Convection in Liquids*. Springer.

POMEAU, Y. 1986 Front motion, metastability and subcritical bifurcations in hydrodynamics. *Physica* D **23**, 3–11.

VAN SAARLOOS, W. & HOHENBERG, P. C. 1992 Fronts, pulses, sources and sinks in generalized complex Ginzburg–Landau equations. *Physica* D **56**, 303–367.

SCHNEIDER, T. M., GIBSON, J. F. & BURKE, J. 2010 Snakes and ladders: localized solutions of plane Couette flow. *Phys. Rev. Lett.* **104**, 104501.

TERAMOTO, T., UEDA, K. & NISHIURA, Y. 2004 Phase-dependent output of scattering process for traveling breathers. *Phys. Rev.* E **69**, 056224.

THUAL, O. & FAUVE, S. 1988 Localized structures generated by subcritical instabilities. *J. Phys. France* **49**, 1829–1833.

TOYABE, K. 2009 Collision dynamics of localized convection cells in binary fluid mixtures: network structure of collision orbit (in Japanese). Master's thesis, Graduate School of Science, Hokkaido University.

WATANABE, T., TOYABE, K., IIMA, M. & NISHIURA, Y. 2010 Time-periodic traveling solutions of localized convection cells in binary fluid mixture. *Theor. Appl. Mech. Japan* **59**, 211–219.

WOODS, P. D. & CHAMPNEYS, A. R. 1999 Heteroclinic tangles and homoclinic snaking in the unfolding of a degenerate reversible Hamiltonian–Hopf bifurcation. *Physica* D **129**, 147–170.